

## STUDY OF STRUCTURAL, ELECTRONIC AND MAGNETIC PROPERTIES OF TRANSITION-METALPEROVSKITE OXIDES $\text{SrMO}_3$ (M = Mn AND Co) BY XRD AND DFT TECHNIQUES

M. MUSA SAAD H.E.\* , A. EL-TAHER

*Department of Physics, College of Science, Qassim University, Buraidah 51452, Saudi Arabia*

In the present study, two interested transition-metal perovskite oxide  $\text{SrMO}_3$  (M = Mn and Co) were prepared by the standard solid-state reaction route. The structural, electronic and magnetic properties were investigated by x-ray powder diffraction (XRD) and full potential linearized muffin-tin orbital (FP-LMTO) method within generalized gradient approximation (GGA) and GGA+U in the framework of density functional theory (DFT). Also, the  $\text{SrMO}_3$  crystals were irradiated in the range 100 – 500 kGy to explore the influence of gamma-radiation on the structural properties of these perovskite oxides. XRD patterns and DFT results showed that all samples were crystallized in a cubic crystal structure (with space group of  $Pm\bar{3}m$  (no. 221) with single phase. The DFT lattice constants are in a good agreement with the experimental results. DFT calculations show strong hybridization between Mn (3d) and Co (3d) and the O (2p) orbitals, and the conduction bands were found to arise from M (3d) – O hybridized orbitals. Partial and total spin magnetic moments were calculated systemically for the  $\text{SrMO}_3$  based on double-exchange interaction  $M^{4+} - O - M^{3+}$ .

(Received October 2, 2016; Accepted December 28, 2016)

*Keywords:* Perovskite oxide; Crystal structure; Physical properties; XRD; DFT

### 1. Introduction

During the last six decades, transition-metal perovskite oxides have been the subject of a large number of experimental and theoretical studies due to their unique physical and chemical properties. For example, ferroelectric character in  $\text{BaTiO}_3$  [1] and multiferroic character in  $\text{BiFeO}_3$  [2], high Curie temperature ( $T_C$ ) in Cr doped strontium ruthenates  $\text{SrRu}_{1-x}\text{Cr}_x\text{O}_3$  [3], p-type electronic conductor properties [4], etc. The scientific interest in transition-metal perovskite oxide materials was derived from their potential technological applications. For example, colossal magnetoresistance (CMR) in  $\text{Pr}_{0.7}\text{Ca}_{0.3}\text{MnO}_3$  [5], spin-filter-type magnetic tunnel junction (MTJ) barriers, such as in  $\text{La}_{0.1}\text{Bi}_{0.9}\text{MnO}_3$  [6], magnetic sensors and memory devices in reading heads, such as in  $\text{SrTiO}_3$  [7,8], electrolytes in solid oxide fuel cells (SOFC), such as in Y doped  $\text{BaCeO}_3$  [9], proton conducting fuel cell (PCFC), such as in  $\text{La}_{0.7}\text{Sr}_{0.3}\text{FeO}_{3-\alpha}$  [10], and so on. Moreover, transition-metal perovskite oxides were reported as materials with half-metallic (HM) and MR characters, such as in pure praseodymium manganites  $\text{PrMnO}_3$  [11], Sr doped praseodymium manganites  $\text{Pr}_{1-x}\text{Sr}_x\text{MnO}_3$  [12], Ca doped lanthanum manganites  $\text{La}_{0.7}\text{Ca}_{0.3}\text{MnO}_3$  [13] and Sr doped lanthanum cobaltites  $\text{La}_{1-x}\text{Sr}_x\text{CoO}_3$  [14], etc.

Perovskite oxide with general chemical formula ( $\text{AMO}_3$ ) has been termed an inorganic changeable oxide due the large flexibility of their crystal structure. Many different inorganic oxides take this or related crystal structure since the parent structure easily distorts or adopt to the relative sizes of A and M ions forming the perovskite oxide  $\text{AMO}_3$ . Consequently, the flexibility of the crystal structure of perovskite oxide  $\text{AMO}_3$  and its ability to accommodate wide range of cations with different ionic sizes and oxidation states in A and M sites are at the origin of the large variety of perovskite oxide based compounds with a wide range of physical properties. The ideal

\* Corresponding author: musa.1964@gmail.com

perovskite oxide  $\text{AMO}_3$  crystallizes in cubic structure; it consists of  $\text{MO}_6$  octahedra connected to each other by corner sharing oxygen, and A cations occupy the 12-fold coordination sites surrounding by eight  $\text{MO}_6$  octahedra. Therefore, the ionic radius of the A ion is larger than that of the M ion and the presence of the different-size cation sites enables a wide variety of perovskite-type oxides. For example, the crystal structures of alkali-earth manganese perovskite oxides  $\text{AMnO}_3$  (A = Ca, Sr, Ba) reflect the importance of size of A site, where the ionic radius of alkali earth ion increases from  $r = 1.98 \text{ \AA}$  for  $\text{Ca}^{2+}$  to  $r = 2.15 \text{ \AA}$  for  $\text{Sr}^{2+}$  and  $r = 2.24 \text{ \AA}$  for  $\text{Ba}^{2+}$ . In this series,  $\text{CaMnO}_3$  crystallizes in an orthorhombic structure derivative of the ideal cubic structure  $\text{SrMnO}_3$  [15], containing intermediately sized ions, crystallizes in both cubic and hexagonal structures and this is rare example of perovskite oxide having alternating crystal structures. While the perovskite oxide  $\text{BaMnO}_3$  exhibits hexagonal structure [16] in which all  $\text{MnO}_6$  octahedra share faces along the  $c$  axis in the crystal. Hexagonal structure in  $\text{SrMnO}_3$  is a 4H-type with alternating face sharing and corner sharing along the  $c$  axis. The hexagonal modification is stabilized up to about  $1035 \text{ }^\circ\text{C}$  where it transferred into an ideal cubic in high temperature [16,17].

In doped manganite perovskite oxides with mixed  $\text{Mn}^{3+}$  ( $3d^4; t_{2g}^3 e_g^1$ ) and  $\text{Mn}^{4+}$  ( $3d^3; t_{2g}^3 e_g^0$ ) valence states, the hopping of  $e_g$  electrons between two partially filled 3d orbitals of neighboring  $\text{Mn}^{3+} - \text{Mn}^{4+}$  ions. This can be simplified by the  $pdd_\sigma$  orbital overlap  $\text{Mn}^{3+} (e_g^1) - \text{O} (2p_\sigma) - \text{Mn}^{4+} (e_g^0)$  and the strong onsite Hund coupling between the  $t_{2g}$  core spins and the  $e_g$  electrons. Such mechanism is known as double exchange (DE) interaction; it brings about simultaneous onset of ferromagnetic (FM) and metallic characters. Besides, there is another mechanism in doped manganite perovskite oxides called antiferromagnetic (AFM) super-exchange (SE) interaction via the  $pdd_\pi$  orbital overlap  $\text{Mn}^{3+} (t_{2g}^4) - \text{O} (2p_\pi) - \text{Mn}^{4+} (t_{2g}^3)$ . Therefore, the presence of FM-DE and AFM-SE interactions along with the presence of disorder plays an important role in determining the electronic and magnetic properties of these doped manganite perovskite oxides. In the present paper, an attempt was made to study the of transition-metal perovskite oxides with the common chemical composition of  $\text{SrMO}_3$  (M = Mn and Co) to investigate the effect of replacement of  $\text{M}^{4+}$ -site with 3d transition-metal ions on the structural, electronic and magnetic properties. Where, the electronic and magnetic results will provide some information on the double-exchange and SE interactions of  $\text{M}^{4+} - \text{O} - \text{M}^{3+}$  in both the  $90^\circ$  and  $180^\circ$  arrangements. Also, to explore the influence of gamma-radiation on the structural properties of the perovskite oxides  $\text{SrMO}_3$  (M = Mn and Co).

## 2. Experimental procedure and details of the calculations

### 2.1. Experimental procedure

The samples with common chemical composition  $\text{SrMO}_3$  (M = Mn and Co) were prepared via the standard solid-state reaction route with initial materials as  $\text{SrCO}_3$ ,  $\text{MnO}_2$  and  $\text{Co}_3\text{O}_4$  with high purity (99.99%). Oxide powder of the starting raw materials were carefully weighed in stoichiometric amount, mixed thoroughly in an agate mortar, before dissolving in acetone followed by milling in a ball-milling machine for 6 h at 500 rpm. Next, the dried powder mixtures were grounded again the samples and pelletized with an organic binder into pellets having a diameter of 15 mm and 2 mm thickness. Then, the dried pellets were calcined at  $1200 \text{ }^\circ\text{C}$  in air for 6 h. The final sintering of the pellets was prepared in the temperature range of  $850 - 900 \text{ }^\circ\text{C}$  for proper densification. To study the effects of gamma-irradiation on the crystal structures of  $\text{SrMO}_3$  samples, they were irradiated with  $\gamma$ -rays obtained from the  $^{60}\text{Co}$  cell. The average dose rate from the  $^{60}\text{Co}$  cell was  $1.0 \text{ Gy/S}$ , and the doses were adjusted to be in the ( $100 \text{ kGy} - 500 \text{ kGy}$ ) range.

The structural characterization of  $\text{SrMO}_3$  (M = Mn and Co) samples was carried out using the x-ray powder diffraction (XRD). The x-ray diffractograms were measured within scan speed of  $2.0^\circ$  per minute, using the continuous scan mode, at ambient temperature by the goniometer type Ultima IV. The instrument is equipped with a copper Cu anode generating Ni filtered  $\text{CuK}\alpha$  radiation ( $\lambda = 1.5406 \text{ \AA}$ ; 40 kV; 40 mA) backmonochromator. The equipment was used in a  $\theta - 2\theta$  scanning angle geometry in the range  $10^\circ - 80^\circ$  with a divergence slit of  $2/3^\circ$ . Here, in the present

study, we will show how can utilize the XRD pattern for determination of many significant parameters of SrMO<sub>3</sub> (M = Mn and Co) samples.

## 2.2. First-principles DFT calculations

Our calculations in this study were based on the first-principles density functional theory (DFT) [18]. The full-potential linearized muffin-tin orbital (FP-LMTO) method working within the atomic plane wave expansion (PLW) [19,20] was used to calculate the physical properties of SrMO<sub>3</sub> (M = Mn and Co). The spin-dependent electronic and magnetic spectra were obtained from the generalized gradient approximation (GGA) [21]. The exchange-correlation parameterization of Perdew-Wang (PW91) [21] were employed in GGA calculations, respectively. Unfortunately, the GGA methods cannot successfully describe the 3d perovskite oxides, so, this deficiency was corrected by adding exchange-correlation terms to GGA by using the GGA+U method [22]. The GGA+U technique yields quite satisfying results for strongly correlated perovskite oxides, so the correlation parameters of Coulomb repulsion (U) and Hund exchange (J) were utilized for the 3d states [23,24]. For transition-metal ions, the near maximum values of U were selected from the reasonable range U = 2.0 eV – 6.0 eV [23–25]. In this study, we employed reasonable values of U = 4.0 eV and J = 0.96 eV, and the settings of these parameters were examined by the total energy convergence reached in the FP-LMTO calculations.

The cutoff energy for PLW basis was set to 450 eV and 6×6×6k-points grids were set in the irreducible part of the Brillouin zone. To find the stable state, the energy convergence criterion for electronic self-consistent calculation was set to 0.001 meV. The Wigner-Seitz radii of the muffin-tin (MT) spheres were set to 2.50, 2.0 and 1.5 a.u. for Sr, M and O atoms, respectively. In addition, the effect of spin-orbit coupling(SOC) was included in GGA and GGA+U calculations by using the scalar relativistic scheme GGA+SOC and GGA+SOC+U based on the Dirac equation [19,20]. The full relativistic effects were calculated within Dirac equation for core states, whereas the scalar relativistic approximation was used for the valence states [26]. Including the SOC effect is important for investigating the electronic and magnetic properties of SrMO<sub>3</sub> (M = Mn and Co) due to the presence of the relatively heavy atoms. The SOC was included in a self-consistent manner by solving the radial Dirac equation for the core electrons and evaluated based on the second variation treatment [26,27]. Thus, the total angular momentum coupled the orbital angular momentum to the spin of the valence and semi-core states of M (3d) in SrMO<sub>3</sub>.

## 3. Results and discussion

### 3.1. Structural properties of SrMO<sub>3</sub>

#### 3.2.1. XRD analysis and gamma-irradiation effect

The measurement of structural parameters using the XRD has therefore many advantages over the other experimental techniques. For example, the XRD does not require time for sample preparation, tinning, and image analyzing. In addition, application of the XRD was done to expose the influence of irradiation on the crystal structure of perovskite oxides. Figures 1 and 2 show the XRD of the SrMO<sub>3</sub> (M = Mn and Co) samples, we can see strong peaks of XRD patterns, which indicate that the SrMO<sub>3</sub> samples are crystallized. The intense peaks in the patterns showed the high crystal structures of these compounds. The relative intensities of the reflection peaks in all patterns agree well with the XRD patterns of bulk perovskite oxides. In addition, the effects of the irradiation on crystal structures of SrMO<sub>3</sub> samples are appeared in the XRD graphs, where clearly changes in the peaks intensities can be observed. The variations of the intensities of the main peaks are due to that the localized variations in the intensities within any individual diffracted spot arise from non-uniformity structural in the lattice planes causing the spot, and this forms the basis for the x-ray topographic technique [28]. This topographic contrast arises from the differences in the intensity of the diffracted beam as a function of the atomic position inside the crystals; therefore, this variation is a function of the crystal structure.

On the other hand, with increasing of the gamma-irradiation doses conduct in the ranges 100 – 300 kGy and 300 – 500 kGy, the crystal structures of SrMO<sub>3</sub> samples were changed in small amounts. From Figures 1 (b) and 1 (b), the 300 kGy shows the preferable dose that can be used in

this respect where at 500 kGy, Figures 1 (c) and 2 (c), the peak intensity is no longer high. Here, if the crystal is strained then the d-spacing will be changed; a compressive stress would make the d-spacing smaller, and the tensile stress would make the d-spacing larger, say reducing the d-spacing to  $d-\delta d$ . Then by using the Bragg's law, the position of the peak will increase from  $2\theta$  to  $2(\theta + \delta\theta)$ . Therefore, if the  $\text{SrMO}_3$  crystals were strained or compressed by an equal amount, they would result in peaks shift from  $2\theta$  to  $2(\theta + \delta\theta)$ . Based on these facts, we can established that all XRD patterns showed the cubic crystal structures with single phase for  $\text{SrMO}_3$  ( $M = \text{Mn}$  and  $\text{Co}$ ) samples. When the samples were irradiated at 300 kGy and 500 kGy, the peaks were influenced and shifted upward. Since the peak-intensity depends mainly on the crystal structure, so we can conclude that the gamma-radiation improved the crystal structures. However, there are roughly decreases in the peaks starting above the 300 kGy. In addition, from Figures 1 and 2 (panels b and c), it can see that the peak positions are the same at 300 kGy and 500 kGy radiation doses, which indicates that the compressive stress in the crystal structures is excepted.

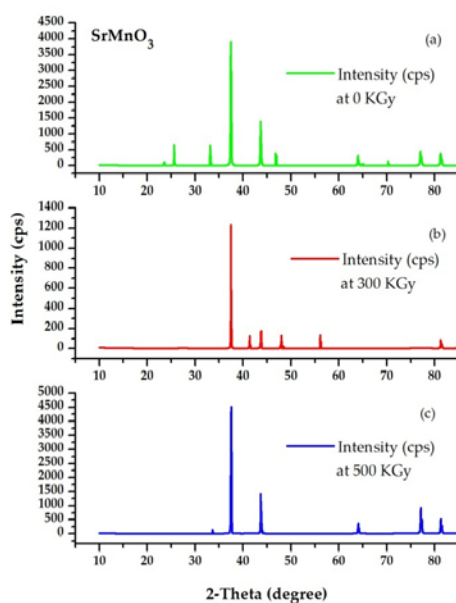


Fig.1. X-ray diffraction patterns for the crystals of perovskite oxide  $\text{SrMnO}_3$  (a) 0, (b) 300, and (c) 500 kGy gamma-irradiation doses

The results of the structural properties of the perovskite oxides  $\text{SrMO}_3$  ( $M = \text{Mn}$  and  $\text{Co}$ ) can be estimated from the XRD patterns plotted in Figures 1 and 2. First, the structural data that summarized in Table 1, the lattice constants and unit cell volumes support that the crystal structures of two compounds are close-packed cubic with space group of  $Pm\bar{3}m$ . Generally, the lattice constants and unit cell volumes are influence by in small amount when the samples are irradiated by exposure of gamma-irradiation. Careful look at these values compared to the pure values leads to conclude that lattice constant values are always more than those values of the standard ones before irradiated the two samples. The irradiated samples show lowest lattice constants of  $a = 3.8074 \text{ \AA}$  for Mn compound whereas  $a = 3.7491 \text{ \AA}$  for Co compound. In addition, according to these results, we concluded that the unit cell volumes increase under the influence of gamma-irradiation dose exposure, and the lowest unit cell volume value was observed at the 300 kGy dose,  $V = 55.193 \text{ \AA}^3$  and  $V = 52.697 \text{ \AA}^3$  for perovskite oxides  $\text{SrMnO}_3$  and  $\text{SrCoO}_3$ , respectively. Therefore, the small fluctuation in the lattice constants and unit cell volumes under different gamma-irradiation doses, as observed in Figures 1 and 2, may be attributed to the variation that occurred of the crystal structures of these compounds due to the effect of irradiation on the particles. These results are in agreement with that observed in doped perovskite oxide  $\text{PrFe}_{1-x}\text{Mn}_x\text{O}_3$  [28] and in pure and doped  $\text{ZnMn}_2\text{O}_4$  spinel structures [29], irradiated by 625-kGy and 100-kGy gamma-irradiation dose, respectively.

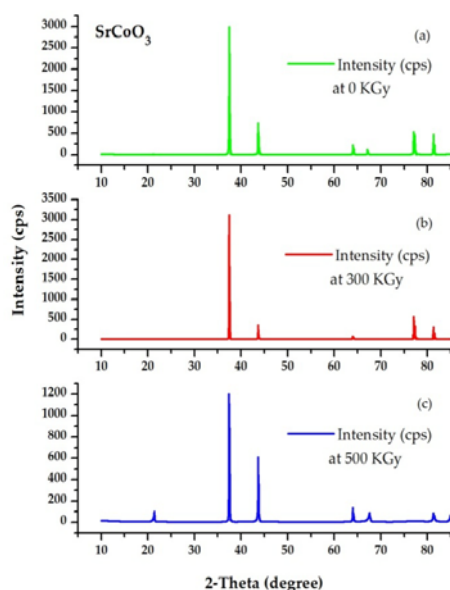


Fig.2. X-ray diffraction patterns for the crystals of perovskite oxide SrCoO<sub>3</sub> at (a) 0, (b) 300, and (c) 500 kGy gamma-irradiation doses.

Table 1. Structural properties of perovskite oxides SrMO<sub>3</sub> (M = Mn and Co) obtained before (0 kGy) and after the samples were irradiated at 300 kGy and 500 kGy

Irradiation dose (kGy)	M = Mn		M = Co	
	<i>a</i> (Å)	<i>V</i> (Å <sup>3</sup> )	<i>a</i> (Å)	<i>V</i> (Å <sup>3</sup> )
0	3.8057	55.113	3.7420	52.398
300	3.8074	55.193	3.7491	52.697
500	3.8077	55.206	3.7495	52.713

### 3.1.2. Rock-salt crystal structure of SrMO<sub>3</sub>

In crystalline material science, if the large oxide ion O<sup>2-</sup> (*R* = 1.40 Å) is combined with a transition-metal having small ionic radius, such Mn<sup>2+</sup> (*R* = 0.67 Å), Co<sup>2+</sup> (*R* = 0.65 Å) and Ni<sup>2+</sup> (*R* = 0.69 Å), the resulting crystal structure can be looked upon as close packed oxygen ions with transition-metal ions in the interstitials. This is observed for many inorganic compounds with oxygen ions and transition-metal of valence +2, e.g. Mn<sup>2+</sup>O<sup>2-</sup>, Co<sup>2+</sup>O<sup>2-</sup> and Ni<sup>2+</sup>O<sup>2-</sup>. In these crystal structures, the O<sup>2-</sup> ions form a cubic close packed (ccp) lattice with the transition-metal ions in the octahedral interstitials, i.e. the rock-salt (Na<sup>+</sup>Cl<sup>-</sup>) structure. Replacing one fourth of the oxygen with a cation of approximately the same radius as O<sup>2-</sup>, e.g. alkali-earth element A (A = Ca<sup>2+</sup>, Sr<sup>2+</sup> or Ba<sup>2+</sup>), reduces the number of octahedral voids, occupied by a small cation M, to one fourth. The resulted chemical formula can be written as AMX<sub>3</sub> and this crystal is represented the perovskite structure. Where the anion X is often O<sup>2-</sup> but also other large ions such as F<sup>-</sup> and Cl<sup>-</sup> are possible. This mineral is stable perovskite type, which is one of the fundamental crystal lattice structures.

Perovskite SrMO<sub>3</sub> is a centrosymmetric solid with a typical cubic perovskite structure in *Pm* $\bar{3}$ *m* space group, in which the Sr<sup>2+</sup> cations are 12-fold coordinated forming cuboctahedral SrO<sub>12</sub> clusters, whereas the M<sup>4+</sup> cations are 6-fold coordinated [30]. The octahedral MO<sub>6</sub> clusters form the framework of the cubic structure, where the Sr<sup>2+</sup>, M<sup>4+</sup> and O<sup>2-</sup> atoms occupy the cube corners and the edge centers, respectively, as shown in Figure 3. From GGA calculations we obtained the equilibrium lattice constants *a* = 3.806 Å for M = Mn, and *a* = 3.74 Å for M = Co, which are in good agreement with previous theoretical data [31,32] as well with the experiments [33–39]. Moreover, similar calculations are repeated by using the GGA+U technique, however the

crystal structure is only slightly changed with respect the GGA one. The lattice constants are calculated to be  $a = 3.806 \text{ \AA}$  for  $M = \text{Mn}$ , and  $a = 3.74 \text{ \AA}$  for  $M = \text{Co}$ . Tables 2 and 3 show the structural properties of the unit cell for perovskite oxides  $\text{SrMO}_3$  ( $M = \text{Mn}^{4+}$  and  $\text{Co}^{4+}$ ). Crystal symmetry, space group (S. G.), lattice constant, unit cell volume, ionic radius, tolerance factor, bond distance and bond angle are obtained from XRD and DFT calculations. Table 4 shows the atomic sites, positions and occupancies of each atom in the ideal unit cell for cubic perovskite oxides  $\text{SrMO}_3$  ( $M = \text{Mn}$  and  $\text{Co}$ ) with  $Pm\bar{3}m$  space group (no. 221).

Table 2. Experimental and DFT calculation of structural properties of perovskite oxides  $\text{SrMO}_3$  ( $M = \text{Mn}$  and  $\text{Co}$ )

$\text{SrMO}_3$	$M = \text{Mn}^{4+}$		$M = \text{Co}^{4+}$	
	Exp.	DFT	Exp.	DFT
Crystal	Cubic	Cubic	Cubic	Cubic
S. G.	$Pm\bar{3}m$	$Pm\bar{3}m$	$Pm\bar{3}m$	$Pm\bar{3}m$
$a$ ( $\text{\AA}$ )	3.8057	3.8060	3.7420	3.7400
$V$ ( $\text{\AA}^3$ )	55.113	55.134	52.398	52.319
$R_M^{4+}$ ( $\text{\AA}$ )	-	0.670	-	0.670
$t$	-	1.0333	-	1.0516

\* The ionic radii of  $\text{Sr}^{2+}$  and  $\text{O}^{2-}$  are  $1.58 \text{ \AA}$  ( $1.44 \text{ \AA}$ ) and  $1.29 \text{ \AA}$  ( $1.44 \text{ \AA}$ )

Table 3. Bond distances (in  $\text{\AA}$ ) and bond angles (in deg.) in cubic  $\text{SrMO}_3$  ( $M = \text{Mn}$  and  $\text{Co}$ )

Cation-bond and multi.	$M = \text{Mn}^{4+}$	$M = \text{Co}^{4+}$
$\text{Sr} (1b)\text{-O} (3d) \times 12$	2.6913	2.6446
$M (1a)\text{-O} (3d) \times 6$	1.9030	1.8700
$\text{O} (3d)\text{-M} (1a)\text{-O} (3d)$	90	90
$M (1a)\text{-O} (3d)\text{-M} (1a)$	180	180

Table 4. Atoms, sites, positions and occupancies for the ideal unit cell of cubic  $\text{SrMO}_3$  ( $M = \text{Mn}$  and  $\text{Co}$ ) with space group of ( $Pm\bar{3}m$ ; no. 221)

atom	Site	position			Occ.
		x	y	z	
Sr	1b	0.5000	0.5000	0.5000	1.0
M	1a	0.0000	0.0000	0.0000	1.0
O	3d	0.0000	0.0000	0.5000	1.0

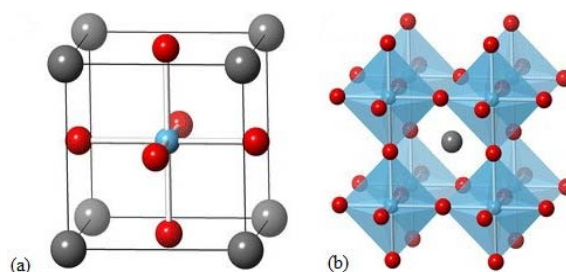


Fig.3. 3D view of the rock-salt structure of perovskite oxide, (a) the unit cell of cubic perovskite oxide  $\text{AMO}_3$ , the A-atoms (brown) form the corners of the cell, M-atoms (blue) are in the center and O-atoms (red) are situated in the faces centers. In (b) the share corners octahedral structure, where the A-atoms occupy every hollow, which is created by eight  $\text{MO}_6$  octahedra, giving the A-atom 12-fold oxygen coordination and the M-atom 6-fold oxygen coordination.

In order to explore the effect of M-site occupation in SrMO<sub>3</sub> crystals, we calculated the structural parameters of these two compounds. Figure 4 shows the relation between the crystal structure parameters, lattice constant, unit cell volume and tolerance factor, and the M-site occupation in perovskite oxides SrMO<sub>3</sub> (M = Mn<sup>4+</sup> and Co<sup>4+</sup>). We calculated these parameters by substituting the M-site with the 3d-ions of Mn<sup>4+</sup> and Co<sup>4+</sup> through increasing of the 3d-occupation in SrMO<sub>3</sub> crystal. We clearly seen that the lattice constant and unit cell volume of SrMO<sub>3</sub> decrease from (a = 3.806 Å and V = 55.134 Å<sup>3</sup>) for M = Mn<sup>4+</sup> (3d<sup>3</sup>; t<sub>2g</sub><sup>3</sup> e<sub>g</sub><sup>0</sup>) to (a = 3.74 Å and V = 52.319 Å<sup>3</sup>) for M = Co<sup>4+</sup> (3d<sup>5</sup>; t<sub>2g</sub><sup>3</sup> e<sub>g</sub><sup>2</sup>). Whereas, the tolerance factor increases from (t = 1.0333) to (t = 1.0516), respectively.

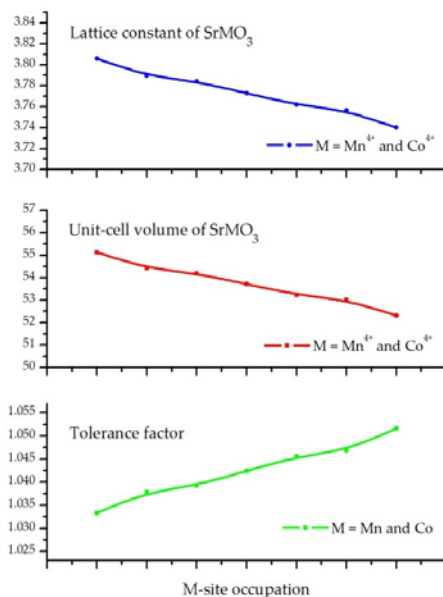


Fig.4. The lattice constants (in Å), unit-cell volumes (in Å<sup>3</sup>) and tolerance factors as function of M-site occupation in perovskite oxides SrMO<sub>3</sub> (M = Mn<sup>4+</sup> and Co<sup>4+</sup>).

### 3.2. Electronic properties of SrMO<sub>3</sub>

In this section, the effect of M-site substitution, spin-orbit coupling (SOC) and exchange-correlation energy on the electronic properties of the perovskite oxides SrMO<sub>3</sub> (M = Mn and Co) are described. Therefore to explain these properties, the total and partial density of states are computed within DFT using different methods GGA, GGA+SOC, GGA+U and GGA+SOC+U, and shown in Figures 5, 6 and 7. They are plotted in the energy range from -8.0 eV to +12.0 eV relative to the Fermi energy. First, in Figure 5, we compare our calculated total density of states (TDOS) of two perovskite oxides SrMO<sub>3</sub> (M = Mn and Co), which are plotted along their high cubic symmetry axes. The large electronic TDOS at Fermi level (E<sub>F</sub>; dash line) in all methods suggests that the proposed compounds have metallic behavior, which is similar with the results obtained by LSDA method [33,36]. There are some bands with different DOS cross the E<sub>F</sub> in both of spin-up and spin-down directions, and therefore no energy-gaps in spin-up and spin-down bands. From GGA and GGA+SOC, it is clearly seen that the TDOS split into three main bands, valence band, between -7.0 eV and -3.0 eV, conduction band through E<sub>F</sub>, between -3.0 eV and +4.0 eV, and a band above E<sub>F</sub>, between +4.0 eV and +11.0 eV. In GGA+U and GGA+SOC+U, Figure 5 (c) and Figure 5 (d), these bands have more splitting due to the U energy. The main contribution in spin-up and spin-down TDOS of SrMO<sub>3</sub> (M = Mn and Co) in the valence bands, between -7.0 eV and -1.0 eV, are mainly due to the Sr (5s), Mn (3d)/ Co (3d) and O (2p) states. The broad O (2p) bands between -3.0 eV and -6.0 eV can be seen to have almost identical structure in both materials, SrMnO<sub>3</sub> and SrCoO<sub>3</sub>, as do the 3d bands, which lie above them. In addition, both bands of Mn (3d) in SrMnO<sub>3</sub> and Co (3d) in SrCoO<sub>3</sub> occupy the same energy levels.

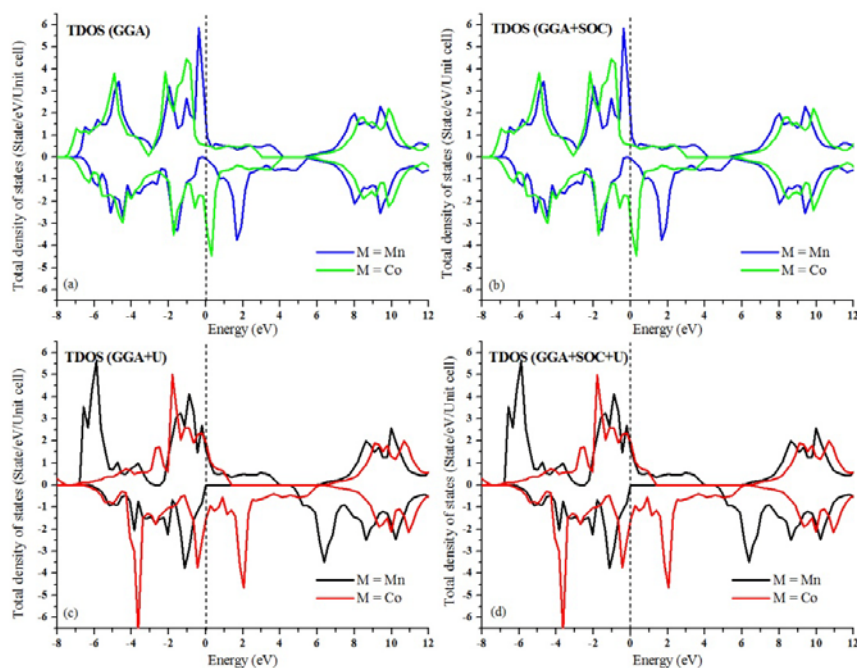


Fig. 5. The total density of states (TDOS) as function of electronic energy for the perovskite oxides  $\text{SrMO}_3$  ( $M = \text{Mn}^{4+}$  and  $\text{Co}^{4+}$ ), computed within DFT using different methods (a) GGA, (b) GGA+SOC, (c) GGA+U and (d) GGA+SOC+U. Fermi level ( $E_F$ ) were set at zero energy and indicated by dash lines.

Moreover, to explain the contribution of different states in the TDOS, the partial density of states (PDOS) of Sr (5s), Mn (3d)/ Co (3d) and O (2p) states for the two perovskite oxides  $\text{SrMO}_3$  with  $M = \text{Mn}$  and  $M = \text{Co}$  are calculated and shows in Figures 6 and 7, respectively. From the GGA and GGA+SOC for  $\text{SrMnO}_3$  in Figures 6 and 7 (a) and (b), the broad O (2p) bands between  $-2.5$  eV and  $-7.0$  eV can be seen clearly with the Mn (3d) and Co (3d) bands above them, which they must place at the turn of the  $E_F$ . Two sharp spin-up and spin-dn peaks of 3.26 and 2.79 expand from  $-1.20$  eV to  $+0.50$  and from  $-0.92$  eV to  $+0.74$  corresponding to the Mn (3d) and Co (3d) states, respectively, are clearly visible through the  $E_F$ . Whereas, these peaks split in spin-up for  $M = \text{Mn}$  and spin-dn for  $M = \text{Co}$  and decline to 2.77 and 0.90, respectively, in PDOS from GGA+U and GGA+SOC+U methods, Figures 6 and 7 (c) and (d). Moreover, in all DOS there is an electronic hybridization between M (3d)/ Co (3d) and O (2p) bands is expected between  $-2.0$  eV and  $+2.0$  eV, and of course leads to the well-known double-exchange interaction in magnetic perovskite oxides.

Once more, we observe the Sr (5s) bands, which can be seen to have considerable dispersion suggesting that it is involved in covalent bonding. In addition, the Mn (3d) and Co (3d) bands overlap with tiny orbitals of partially occupied Sr (5s) states. The large TDOS at the  $E_F$  for these compounds suggests that the cubic FM structure is stable, and that a lower energy structure could be achieved by allowing spin-polarization of the conduction electron. The TDOS and projected PDOS of  $\text{SrMnO}_3$  are similar to previously published ones [37,40,41], and agree well with the experiment [31,42]. The top of the valence band is composed of O (2p) – Mn (3d) and O (2p) – Co (3d) hybridized orbitals, while the bottom of conduction band is mainly composed of Mn (3d) and Co (3d) orbitals, see Figures 6 and 7. The modest contribution of the Sr (5s) orbitals is located in the middle of the top of the valence bottom of conduction bands. For  $\text{SrMnO}_3$ , the calculated energy-gap in spin-dn band is 0.52 eV, Figure 6, which compares well with previously reported value, i.e. 0.75 eV [40]. The underestimation with respect to the experimental values of 3.2–3.4 eV [31,42] is a well-known consequence of the incomplete cancellation of the self-interaction in the local exchange functional of the GGA. Moreover, similar calculations are repeated by using the GGA+U and GGA+SOC+U techniques for perovskite oxides  $\text{SrMO}_3$  ( $M =$

Mn and Co). However, the energy-gap is only considerably changed with respect the GGA and GGA+SOC methods, the energy-gap is calculated to be 4.51 eV for  $M = \text{Mn}$ , which is significantly increased, while for  $M = \text{Co}$ , there is a tiny spin-up band cross the  $E_F$  and two splitting spin-down bands around the  $E_F$ . The Co results in  $\text{SrCoO}_3$  are agreement with the previous published ones [43,44]. In addition, no significant changes appear in the TDOS and PDOS shapes for two compounds.

Furthermore, clearly, the PDOS for Mn (3d) and Co (3d) states are expanded and responsible for the metallic behavior of the perovskite oxides  $\text{SrMnO}_3$  and  $\text{SrCoO}_3$ , respectively. Since the 3d orbitals split into  $t_{2g}$  and  $e_g$  states, the  $3d-t_{2g}$  states are more localized than the  $3d-e_g$  states. Thus, the  $M(3d-e_g) - O(2p)$  bond in  $\text{SrMnO}_3$  is stronger as compared with the  $M(3d-t_{2g}) - O(2p)$ . Consequently, the partial states of  $M(3d-e_g)$  and  $O(2p)$  hybridizes and cross the  $E_F$  in the electronic TDOS, due to which, the perovskite oxides show metallic behavior. It is also clear that  $M(3d-t_{2g})$  and  $M(3d-e_g)$  in GGA+U and GGA+SOC+U results, Figures 6 and 7 (c) and (d), are shifted toward the valence bands as compared to GGA and GGA+SOC, which is due to the fact that GGA method is not appropriate to treat 3d states exactly.

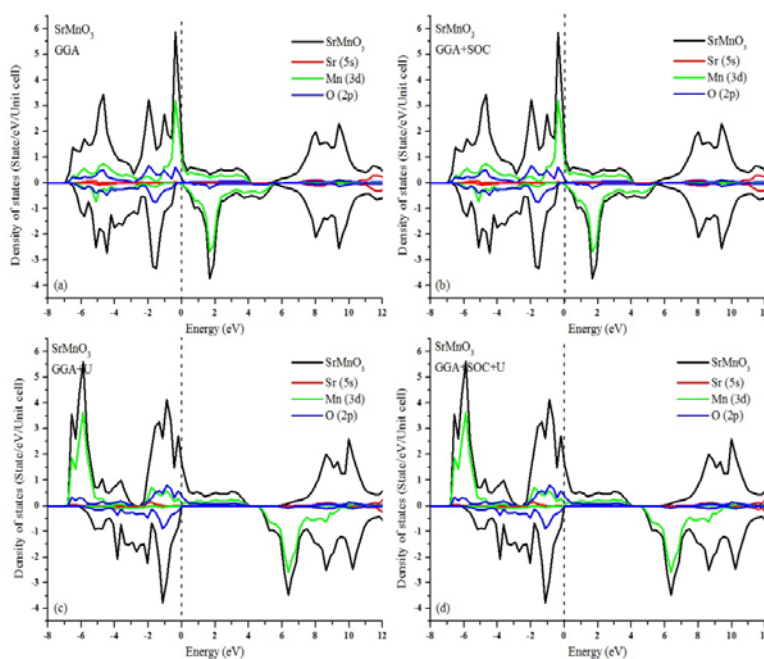


Fig. 6. The total and partial [Sr (5s), Mn (3d) and O (2p)] density of states as function of electronic energy for the perovskite oxide  $\text{SrMnO}_3$ , computed within DFT using different methods (a) GGA, (b) GGA+SOC, (c) GGA+U and (d) GGA+SOC+U. Fermi level ( $E_F$ ) were set at zero energy and indicated by dash lines.

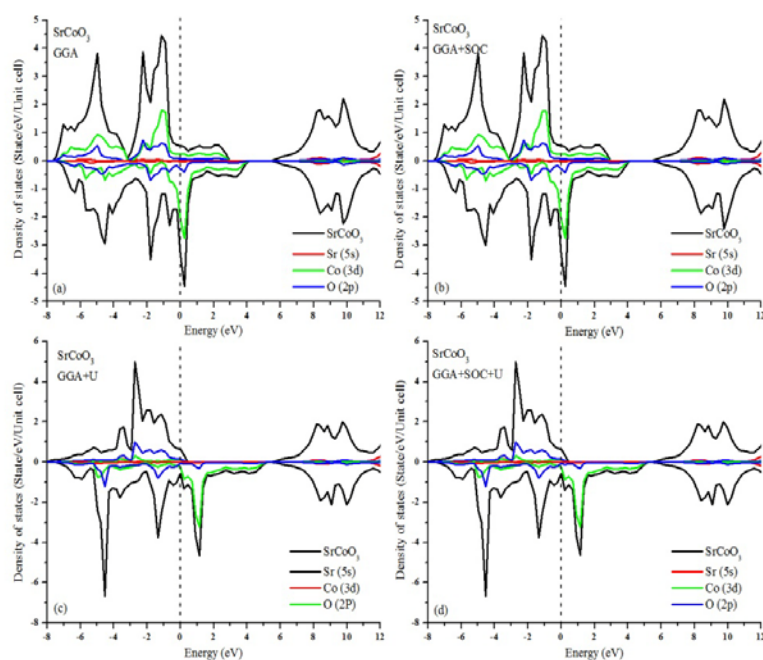


Fig. 7. The total and partial [Sr (5s), Co (3d) and O (2p)] density of states as function of electronic energy for the perovskite oxide  $\text{SrCoO}_3$ , computed within DFT using different methods (a) GGA, (b) GGA+SOC, (c) GGA+U and (d) GGA+SOC+U. Fermi level ( $E_F$ ) were set at zero energy and indicated by dash lines.

### 3.3. Magnetic properties of $\text{SrMO}_3$

In order to describe the magnetic properties of transition-metal perovskite oxides, we first investigate the magnetic interaction and its mechanisms in these materials. As is well known, double-exchange (DE) is a type of a magnetic interaction that was originally proposed by C. Zener [45] for FM manganites with perovskite oxide structure. Then it applied to  $\text{SrMO}_3$  by K. Kubo and N. Ohata [46] to account for the simultaneous appearance of its FM order and metallic behavior. To describe DE mechanism in perovskite oxides  $\text{SrMO}_3$  ( $M = \text{Mn}$  and  $\text{Co}$ ), a little must first be understood about the electronic and magnetic structures about the transition-metals Mn (3d) and Co (3d) sites. In an ideal crystal lattice, the 3d orbital splits into two sub-states, a triple  $t_{2g}$  and double  $e_g$  sub-orbitals, due to the crystal field created by the cubic symmetry surrounding the M (3d) sites with  $\text{Mn}^{4+}$  ( $3d^3$ ;  $t_{2g}^3 e_g^0$ ) and  $\text{Co}^{4+}$  ( $3d^3$ ;  $t_{2g}^3 e_g^2$ ). The doublet  $e_g$  sub-orbitals in  $\text{SrMO}_3$  usually lay 2–4 eV above the triplet  $t_{2g}$  sub-orbitals in energy, see Fig. 8.

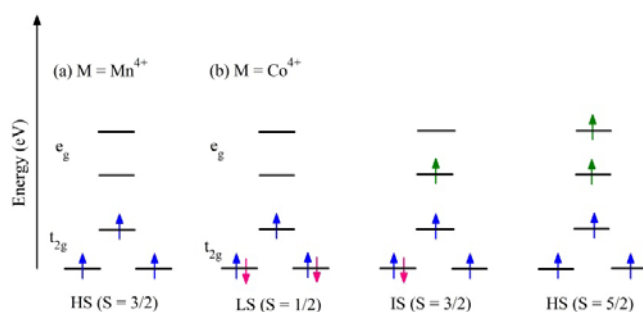


Fig. 8. Splitting of 3d levels into  $t_{2g}$  and  $e_g$  substates due to the octahedral crystal field and different possible spin states for (a)  $\text{Mn}^{4+}$  ( $3d^3$ ) and (b)  $\text{Co}^{4+}$  ( $3d^3$ ) in  $\text{SrMO}_3$  ( $M = \text{Mn}$  and  $\text{Co}$ ).

In octahedral crystal field,  $\text{Mn}^{4+}$  ( $3d^3$ ) ions have only one possible spin state,  $t_{2g}^3 e_g^0$  ( $S = 3/2$ ) with three unpaired electrons, whereas  $\text{Co}^{4+}$  ( $3d^5$ ) ions have three possible spin states,  $t_{2g}^5 e_g^0$  ( $S = 1/2$ ),  $t_{2g}^4 e_g^1$  ( $S = 3/2$ ) and  $t_{2g}^3 e_g^2$  ( $S = 5/2$ ) with one, three and five unpaired electrons, respectively. We designated these spin states in Figure 8 as low spin (LS) state with one unpaired electron, intermediate spin (IS) state with two or three unpaired electrons and high spin (HS) state with five unpaired electrons for  $\text{Mn}^{4+}$  and  $\text{Co}^{4+}$  ions. These spin state configurations of  $\text{Mn}^{4+}$  ( $3d^3$ ) and  $\text{Co}^{4+}$  ( $3d^5$ ) ions in octahedral crystal field are schematically represented in Fig. 8.

Moreover, the Coulomb-repulsion energy  $U$  forces each 3d-electron to lay on a lonely level, and the Hund's rule coupling is strong enough to ensure that all 3d electrons on the Mn (3d) and Co (3d) sites are FM aligned. In Mn (3d) ions, three electrons drive to fill the lower lying  $t_{2g}^3$  states forming an inert core-spin of  $S = 3/2$ , whereas the remaining electrons lie in a superposition of the  $e_g^0$  states. While in Co (3d) ions, also three electrons drive to fill the  $t_{2g}^3$  states forming  $S = 3/2$  and the remaining electrons lie in the  $e_g^2$  states. These electrons may move through the lattice subject to the constraint, that the hopping-electron always has its spin aligned with its host's core-spin. The hopping from  $\text{Mn}^{4+}$  to  $\text{Mn}^{3+}$  or  $\text{Co}^{4+}$  to  $\text{Co}^{3+}$  is mediated by the  $\text{O}^{2-}$  ions between them, and DE organizes this hopping interaction. As the temperature is lowered and spin fluctuations decreased, the crystal lowers its energy by FM aligning the M (3d) core-spins allowing the  $e_g$  electrons to gain kinetic energy and move about the crystal. The hopping transfer integral calculated from such DE theory is a very sensitive function of the  $\text{M}^{4+} - \text{O} - \text{M}^{3+}$  bond angle, deviation from the ideal  $180^\circ$  resulting in much reduced hopping probability. This agrees with experimental evidence, where different divalent dopants with different atomic radii cause about large change in the Curie temperature ( $T_C$ ). Dopants with small atomic radii cause a buckling in the  $\text{M}^{4+} - \text{O} - \text{M}^{3+}$  bond angle, decreasing the single electron bandwidth and consequently reducing the  $T_C$ . The effect of dopant size on the structural and electronic properties can be described using the tolerance factor, which describes the degree of deviation from ideal cubic symmetry, as we discussed it extensively in section 3.1.2 for crystal structure properties.

Table 5. Spin magnetic moments (in  $\mu_B$ ) in cubic  $\text{SrMO}_3$  ( $M = \text{Mn}$  and  $\text{Co}$ ), calculated using GGA, GGA+SOC, GGA+U and GGA+SOC+U within DFT method.

DFT method	GGA	GGA+SOC	GGA+U	GGA+SOC+U
<b>SrMnO<sub>3</sub></b>				
Sr (5s)	0.0669	0.0669	0.0251	0.0251
Mn (3d)	2.4768	2.4768	3.6688	3.6688
O (2p)	0.3037	0.3037	-0.7828	-0.7828
Total	2.6450	2.6451	3.4330	3.4330
<b>SrCoO<sub>3</sub></b>				
Sr (5s)	0.0589	0.0590	0.0593	0.0593
Co (3d)	1.6519	1.6523	3.4630	3.4629
O (2p)	0.5422	0.5430	1.0808	1.0809
Total	2.2530	2.2543	3.8826	3.8825

Then, the magnetic properties of perovskite oxides  $\text{SrMO}_3$  ( $M = \text{Mn}$  and  $\text{Co}$ ) were investigated in detailed, where the spin magnetic moments were calculated by using the four different approximations; GGA, GGA+SOC, GGA+U and GGA+SOC+U, within DFT method. Table 4 shows the calculated partial and total spin magnetic moments for the cubic symmetry in two compounds. First, we remark that when we used the Coulomb repulsion energy  $U$ , the obtained spin magnetic moments have extensive increase, whereas the SOC term has small effect. We see clearly from these results, the spin magnetic moments are overestimated by both GGA+U and GGA+SOC+U methods, but less that the GGA+U calculation gives the biggest values, especially the partial spin magnetic moments of Mn (3d) and Co (3d) ions, which are more important than others. The electronic configuration of the Mn ( $Z = 25$ ) and Co ( $Z = 27$ ) atoms are  $[\text{Ar}]^{18} 3d^5 4s^2$  and  $[\text{Ar}]^{18} 3d^7 4s^2$ , respectively, which indicate the dissimilar configurations of these elements in their compounds. The obtained values are  $3.6688 \mu_B$  for  $M = \text{Mn}$  (3d) and  $3.4630 \mu_B$  for  $M = \text{Co}$  (3d), which suggest the electronic configuration of the 3d ions in-between  $\text{Mn}^{4+}$

( $3d^3$ ) and  $Mn^{3+}$  ( $3d^4$ ) and  $Co^{4+}$  ( $3d^5$ ) and  $Co^{3+}$  ( $3d^6$ ) states in  $SrMnO_3$  and  $SrCoO_3$ , respectively. Our results agree very well with the calculated partial and total spin magnetic moments of perovskite oxides  $SrMnO_3$  and  $SrCoO_3$ , performed by using GGA method [16,47,48]. In those studies, it carried out the values of  $2.50 \mu_B$  and  $2.967 \mu_B$ , respectively, for the FM configuration of the cubic structure.

On the other hand, the spin magnetic moment of the  $O^{2-}$  ions is very small; approximately equal to zero in two compounds, with small contribution to the total spin magnetic moment. The same remark is revealed for the  $Sr^{2+}$  ions, we found that its spin magnetic moment is negligibly smaller than the other ions in each of  $SrMnO_3$  and  $SrCoO_3$ . Moreover, both GGA and GGA+SOC calculations produce similar results for the M (3d) ions, around  $2.5 \mu_B$  and  $1.7 \mu_B$  for  $M = Mn$  and for  $M = Co$ , respectively, whereas the GGA+U and GGA+SOC+U calculations overestimated the spin magnetic moment of the M (3d) ions, in comparison with the obtained values from GGA and GGA+SOC. The GGA+U and GGA+SOC+U calculations give the bigger values than GGA and GGA+SOC ones, which show the effect of U parameter, especially on the spin magnetic moment of the M (3d) ions. Thus, the exchange-correlation methods, GGA+U and GGA+SOC+U, are more accurate than others used in the calculations, which they will be indispensable for the electronic and magnetic structure calculations, particularly for the transition-metal materials.

#### 4. Conclusions

In summary, the structural, electronic and magnetic properties of two interested transition-metal perovskite oxides  $SrMO_3$  ( $M = Mn$  and  $Co$ ) were investigated by x-ray powder diffraction (XRD) and full potential linearized muffin-tin orbital (FP-LMTO) method within generalized gradient approximation (GGA) and GGA+U based on the density functional theory (DFT). First, the effect of the gamma-irradiation on the crystal structures of perovskite oxides  $SrMO_3$  ( $M = Mn$  and  $Co$ ) was explored in the range of 100 kGy – 300 kGy dose.

We found that there are small change in the structural parameters of  $SrMO_3$  ( $M = Mn$  and  $Co$ ) after they irradiated. The XRD and DFT results showed that all samples were crystallized in a cubic crystal structure with single phase. Second, the structural properties of these perovskite oxides were investigated theoretically, which showed cubic symmetry with space group of  $Pm\bar{3}m$  (no. 221). The increasing of the occupation number of M-site in perovskite oxides  $SrMO_3$  ( $M = Mn^{4+}$  and  $Co^{4+}$ ) decreased the lattice constant and unit cell volume, while it increased the tolerance factor of  $SrMO_3$ . Then the electronic properties of perovskite oxides  $SrMO_3$  ( $M = Mn$  and  $Co$ ) were investigated by calculating the total (TDOS) and partial (PDOS) density of states of these two compounds using GGA, GGA+SOC, GGA+U and GGA+SOC+U methods. Electronic TDOS there are some bands with different DOS cross the  $E_F$  in spin-up and spin-down directions. We found that the PDOS of Mn (3d) and Co (3d) states, which hybridize with O (2p) states, are responsible for the metallic behavior of the perovskite oxides  $SrMnO_3$  and  $SrCoO_3$ , respectively.

Finally, the magnetic properties of transition-metal perovskite oxides  $SrMO_3$  ( $M = Mn^{4+}$  and  $Co^{4+}$ ) were investigate in details. Also, the possible spin states of  $Mn^{4+}$  ( $3d^3$ ) and  $Co^{4+}$  ( $3d^5$ ) ions in octahedral crystal field was discussed, where  $Mn^{4+}$  ( $3d^3$ ) splitting into  $t_{2g}^3 e_g^0$  ( $S = 3/2$ ) with three unpaired electrons, whereas  $Co^{4+}$  ( $3d^5$ ) have  $t_{2g}^5 e_g^0$  ( $S = 1/2$ ),  $t_{2g}^4 e_g^1$  ( $S = 3/2$ ) and  $t_{2g}^3 e_g^2$  ( $S = 5/2$ ) with one, three and five unpaired electrons, respectively. The magnetic double-exchange interaction  $M^{4+} - O - M^{3+}$  and its mechanisms in  $SrMO_3$  materials were described. The partial and total spin magnetic moments for the cubic symmetry in two compounds  $SrMO_3$  ( $M = Mn^{4+}$  and  $Co^{4+}$ ) were calculated by using the four different approximations, GGA, GGA+SOC, GGA+U and GGA+SOC+U, within the DFT method.

#### Acknowledgments

The authors gratefully acknowledge Qassim University (QU), Saudi Arabia, represented by the Deanship of Scientific Research, on the material support for this research under the Grand number (3000) during the academic year 1436 AH / 2015 AD.

## References

- [1] Ronald E. Cohen, Origin of ferroelectricity in perovskite oxides, *Nature* **358**, 136 (1992).
- [2] J.B. Neaton, C. Ederer, U.V. Waghmare, N.A. Spaldin, K.M. Rabe, *Phys. Rev. B* **71**, 014113 (2005).
- [3] Li Pi, A. Maignan, R. Retoux, B. Raveau, *J. Phys.: Condens. Matter* **14**, 7391 (2002).
- [4] Junichiro Mizusaki, *Solid State Ionics* **52**(1–3), 79 (1992).
- [5] Joonghoe Dho, W.S. Chim, E.O. Chi, N.H. Hur, S.H. Park, H.-C. Ri, *Solid State Communications* **125**(3–4), 143 (2003).
- [6] Martin Gajek, Manuel Bibes, Stéphane Fusil, Karim Bouzehouane, Josep Fontcuberta, Agnès Barthélémy, Albert Fert, *Nature Materials* **6**, 296 (2007).
- [7] Run-Wei Li, *Int. of Nanotechnology* **6**(12), 1067 (2009)5.
- [8] Jeffery W. Fergus, *Sensors and Actuators B: Chemical* **123**(2), 1169 (2007).
- [9] N. Bonanos, K.S. Knight, B. Ellis, *Solid State Ionics* **79**, 161 (1995).
- [10] Hiroyuki Yamaura, Tetsuya Ikuta, Hidenori Yahiro, Genji Okada, *Solid State Ionics* **176**(3–4), 269 (2005).
- [11] B. Bouadjemi, S. Bentata, A. Abbad, W. Benstaali, B. Bouhafs, *Solid State Communications* **168**, 6 (2013).
- [12] J.-S. Kang, T.W. Noh, C.G. Olson, B.I. Min, *Journal of Electron Spectroscopy and Related Phenomena* **114–116**, 683 (2001).
- [13] J.Y.T. Wei, N.-C. Yeh, R.P. Vasquez, *Physical Review Letters* **79**, 25, (1997).
- [14] Ying-Ni Duan, Xiao-Xi Fan, Abdugheni Kutluk, Xiu-Juan Du, Yu-Ling Song, *Journal of Magnetism and Magnetic Materials* **384**, 229 (2015).
- [15] F. F. Fava, P. D'Arco, R. Orlando, R. Dovesi, *J. Phys.: Condens. Matter* **9**, 489 (1997).
- [16] Rune Søndena, Svein Stølen, P. Ravindran, Tor Grande, Neil L. Allan, *Phys. Rev. B* **75**, 184105 (2007).
- [17] L. Rørmark, A. B. Mørch, K. Wiik, S. Stølen, T. Grande, *Chem. Mater.* **13**, 4005 (2001).
- [18] P. Hohenberg, W. Kohn, *Inhomogeneous Electron Gas*, *Phys. Rev.* **136** (3B), 864 (1964); W. Kohn, L.J. Sham, *Phys. Rev.* **140**(4A), 1133 (1965).
- [19] S. Y. Savrasov, *Phys. Rev. B* **54**, 16470 (1996).
- [20] S. Yu. Savrasov, D. Yu. Savrasov, *Phys. Rev. B* **46**, 12181 (1992).
- [21] John P. Perdew, Yue Wang, *Phys. Rev. B* **45**, 13244 (1992).
- [22] Zhongqin Yang, Zhong Huang, Ling Ye, Xide Xie, *Phys. Rev. B* **60**, 15674 (1999).
- [23] X. F. Zhu, Q. F. Li, L. F. Chen, *J. Phys.: Condens. Matter* **20**, 075218 (2008).
- [24] Antonis N. Andriotis, R. Michael Sheetz, Madhu Menon, *Phys. Rev. B* **81**, 245103 (2010).
- [25] M. Musa Saad H.-E., *J. Alloys Compd.* **587**, 652 (2014).
- [26] A. H. MacDonald, W. E. Pickett, D. D. Koelling, *J. Phys. C: Solid State Phys.* **13**, 2675 (1980).
- [27] T. Takeda, *Z. Physik B* **32**, 43 (1978).
- [28] M. Khairy, M. A. Mousa, *Phys. Chem.* **2**(6), 109 (2012).
- [29] Khalid Sultan, M. Ikram, K. Asokan, *AIP Conf. Proc.* **1591**, 1278 (2014),
- [30] Haiwei Du, Xi Lin, Zhemi Xu, Dewei Chu, *Journal of Materials Science* **50**(17), 5641 (2015).
- [31] H. Sakai, S. Ishiwata, D. Okuyama, A. Nakao, H. Nakao, Y. Murakami, Y. Taguchi, Y. Tokura, *Phys. Rev. B* **82**, 180409(R) (2010).
- [32] Rune Søndena, P. Ravindran, Svein Stølen, Tor Grande, Michael Hanfland, *Phys. Rev. B* **74**, 144102 (2006).
- [33] T. Takeda, S. Ohara, *J. Phys. Soc. Jpn.* **37**, 275, (1974).
- [34] O. Chmaissem, B. Dabrowski, S. Kolesnik, J. Mais, D. E. Brown, R. Kruk, P. Prior, B. Pyles, J. D. Jorgensen, *Phys. Rev. B* **64**, 134412, (2001).
- [35] T. Negas, R. S. Roth, *J. Solid State Chem.* **1**, 409, (1970).
- [36] Haiping Wu, Weishi Tan, Chuanyun Xiao, Decai Huang, Kaiming Deng, Yan Qian, *Solid State Communications* **151**, 1616 (2011).
- [37] Xing-Yuan Chen, Wei-ling Zhu, Shi-Yuan Lin, Yu-Jun Zhao, *Computational Materials Science* **83**, 394 (2014).
- [38] Sun Aimin, Zhang Xiu'e, Kang Yonggang, Yang Guofeng, Wang Shunqing, Zhang Tao,

- Huang Guohai, Zhu Haibin, *Physica B* **403**,1927 (2008).
- [39] Jian Ni, *Physica B* **405**,3638 (2010)
- [40] D. Fuks, S. Dorfman, J. Felsteiner, L. Bakaleinikov, A. Gordon, E.A. Kotomin, *Solid State Ionics* **173**, 107 (2004).
- [41] Hanghui Chen, Hyowon Park, Andrew J. Millis, Chris A. Marianetti, *Phys. Rev. B* **90**,245138 (2014).
- [42] A. Sacchetti, M. Baldini, P. Postorino, C. Martin, A. Maignan, *Journal of Raman Spectroscopy* **37**(5),591 (2006).
- [43] M. Zhuang, W. Y. Zhang, A. Hu, N. B. Min, *Phys. Rev. B* **57**, 13655 (1998),.
- [44] Taguchi, H., Shimada, M. & Koizumi, *Mater. Res. Bull.* **13**, 1225 (1978).
- [45] Clarence Zener, *Phys. Rev.* **82**, 403 (1951).
- [46] Kenn Kubo, Nagao Ohata, *J. Phys. Soc. Jpn.* **33**, 21 (1972).
- [47] Y. Long, Y. Kaneko, S. Ishiwata, Y. Taquchi, Y. Tokura, *J. Phys. Condens. Matter.* **23**(24), 245601 (2011),.
- [48] Guang Song, Weiyi Zhang, *Scientific Reports* **4**,4564 (2014).